


Tracking iron oxide nanoparticles in plant organs using magnetic measurements

E. Govea-Alcaide · S. H. Masunaga  · A. De Souza ·
L. Fajardo-Rosabal · F. B. Effenberger · L. M. Rossi ·
R. F. Jardim

Received: 7 July 2016 / Accepted: 27 September 2016 / Published online: 10 October 2016
© Springer Science+Business Media Dordrecht 2016

Abstract Common bean plants were grown in soil and irrigated with water solutions containing different concentrations of Fe_3O_4 nanoparticles (NPs) with a mean diameter close to 10 nm. No toxicity on plant growth has been detected as a consequence of Fe deficiency or excess in leaves. In order to track the Fe_3O_4 NPs, magnetization measurements were performed in soils and in three different dried organs of the plants: roots, stems, and leaves. Some magnetic features of both temperature and magnetic field

dependence of magnetization $M(T, H)$ arising from Fe_3O_4 NPs were identified in all the three organs of the plants. Based on the results of saturation magnetization M_s at 300 K, the estimated number of Fe_3O_4 NPs was found to increase from 2 to 3 times in leaves of common bean plants irrigated with solutions containing magnetic material. The combined results indicated that $M(T, H)$ measurements, conducted in a wide range of temperature and applied magnetic fields up to 70 kOe, constitute a useful tool through which the uptake, translocation, and accumulation of magnetic nanoparticles by plant organs may be monitored and tracked.

E. Govea-Alcaide · A. De Souza
Departamento de Matemática-Física, Facultad de Ciencias
Informáticas, Naturales y Exactas, Universidad de
Granma, Apdo. 21, P. O. Box 85100, Bayamo, Cuba
e-mail: egoveaa@udg.co.cu

S. H. Masunaga (✉) · R. F. Jardim
Instituto de Física, Universidade de São Paulo, Rua do
Matão, 1371, São Paulo, SP CEP 05508-090, Brazil
e-mail: sueli.masunaga@gmail.com

L. Fajardo-Rosabal
Centro de Estudios de Biotecnología Vegetal, Facultad de
Ciencias Agrícolas, Universidad de Granma, Apdo. 21,
P. O. Box. 85100, Bayamo, Cuba

F. B. Effenberger
Departamento de Engenharia Química, Centro
Universitário FEI, Av. Humberto de A. C. Branco 3972,
S. B. Campo, São Paulo 09850-901, Brazil

L. M. Rossi
Instituto de Química, Universidade de São Paulo,
CP 26077, São Paulo, SP 05513-970, Brazil

Keywords Common bean plants · Fe_3O_4
nanoparticles in soil · Uptake, translocation, and
accumulation of magnetic nanoparticles by plant
organs · Nanobiotechnology

Introduction

Iron and zinc deficiencies are some of the most common nutritional disorders in human beings (Welch and Graham 1999). Among major crop species, legumes are a good source of the above-mentioned micronutrients (Wang et al. 2003). In common bean (*Phaseolus vulgaris* L.), by far the most important grain legume in the world (Broughton et al. 2003), the iron concentration ranges from ~30 to 120 ppm

(Graham and Welch 1999). From the social point of view, common bean is important not only for its nutritional quality but also for poverty alleviation in both developed and developing countries.

Micronutrients such as iron and zinc are taken up by the roots of plants from the soil and transferred through vascular transport to the seeds (Grusak 2002). The uptake, translocation, and accumulation of micronutrients may be enhanced by using magnetic nanoparticles (MNPs) in order to improve the concentration of iron and other chemical elements in edible organs of plants, a process also referred to as biofortification (Welch and Graham 2004). However, it is widely accepted that our knowledge of the biological effects of NPs is still incomplete, because the impact of nanomaterials on plants depends on several parameters such as the type, size, and functionalization of NPs, the plant species, and the plant substrate (Arruda et al. 2015). Some interesting approaches to this matter are found in Schwab et al. (2016) and Servin et al. (2015). In addition, it is indispensable to have an effective control of the unfavorable effects of NPs to the soil, water, and to the environmental pollution in agriculture (Chen et al. 2014).

The large surface area in leaves and root structures of many plant species suggest that plants may have a large potential to interact with NPs. One of the most important distinctive features of plant cells is that they are enclosed by rigid cell walls composed of cellulose, hemicelluloses, and pectin with pores whose diameter is typically in the range of 3–8 nm allowing only small molecules to pass through them (Carpita and Gibeault 1993). Therefore, some authors hypothesized that only NPs with a mean diameter smaller than the pores of the cell walls may travel through and reach the plasma membrane (Navarro et al. 2008). Also, many studies have indicated that not only small NPs, such as TiO_2 and Au with diameters of <5 nm (Kurepa et al. 2010), but also larger NPs were taken up by plant roots or even transported into the plant aerial organs (Corredor et al. 2009). However, it is still unclear in which route the nanoparticles pass through the cell walls and are internalized by the plant cells to undergo vascular transport in plants, or how these particles pass through the Casparian strip (Roppolo et al. 2011).

On the other hand, some experimental results suggest that NPs may diffuse from soil to the roots by several processes as osmotic pressure, capillary

forces, pores across the cell wall (thickness ranging from 5 to 20 nm) (Fleischer et al. 1999), the intercellular plasmodesmata (50–60 nm at midpoint) (Lin and Xing 2008), or via the highly regulated symplastic route (Roberts and Oparka 2003). Other possible routes of NPs uptake would include traversing the cuticle surface of leaves, the cuticle-free portions of the plant (e.g., flowers), suberin-coated roots, or regions of new root formation, and also injured areas (Maurer-Jones et al. 2013). Studies about NPs uptake by plants and their transport inside living plants are still not conclusive for all nanomaterials (Servin et al. 2015).

We finally mention that the production and use of nanoparticles have been increasing considerably, increasing the possibility of releasing these substances into the environment, either intentionally or accidentally (López-Moreno et al. 2016; Schiavo et al. 2016). Therefore, monitoring the NPs fate and toxicity in plants are of paramount importance to human health and environmental risks of nanomaterials (Barrios et al. 2016). Moreover, tracking the uptake, translocation, and accumulation processes of engineered NPs from soil to plant organs, and thus to the food chain, constitute an important task for researchers of diverse fields of science such as physics, chemistry, biology, agriculture, and others (Rico et al. 2011). Also, few studies have been conducted on edible plants by using Fe_3O_4 NPs (Zhu et al. 2008; Barrena et al. 2009; Zahra et al. 2015; López-Luna et al. 2016). In the pioneer work on this particular subject, the authors studied the uptake, translocation, and accumulation of Fe_3O_4 NPs, with mean diameter ~ 20 nm, in pumpkin seedlings grown in hydroponic conditions (Zhu et al. 2008). Furthermore, they conducted a similar study in plants grown in sand and soil, and have detected a much lower level of MNPs uptake and accumulation for the former, and found a non-detectable magnetic signal in the latter. These results were ascribed to the adherence of the MNPs to the soil and sand grains (Zhu et al. 2008). In summary, a systematic study of the uptake, translocation, and accumulation of Fe_3O_4 NPs in plants grown in soils and tracked by magnetic measurements is still lacking in the literature.

Here we report the first systematic study, to our knowledge, of the uptake, translocation, and accumulation of magnetite Fe_3O_4 NPs of ~ 10 nm by common bean plants grown in soil. A set of magnetization data as a function of temperature $M(T)$ and

magnetic field $M(H)$, taken in a broad temperature range from 5 to 300 K and under magnetic fields up to ± 70 kOe, is discussed. The magnetic signals measured in roots, stems, and leaves clearly indicate an uptake of magnetite NPs by the common bean plants from the soil and their subsequent accumulation in the plant organs.

Experimental procedure

Certified common bean (*Phaseolus vulgaris* L.) seeds were used to grow the plants in a soil media using three polyethylene bags, with two replications each, which were identified as *B0*, *B1*, and *B2*. Bags *B1* and *B2* were irrigated daily with 20 mL of water and 20 mL of suspended Fe_3O_4 NPs with concentrations of 1000 and 2000 mg/L, respectively. The seeds in the bag *B0* (control) were grown in a soil free of Fe_3O_4 NPs and irrigated daily with 40 mL of pure water. The experiments were conducted in a set of three plants irrigated with water containing different concentrations of Fe_3O_4 nanoparticles. Also, the plants were grown at the University of Granma (20.281°N, 72.724°W, 210 m asl), located in Bayamo city, Cuba. The growth of the common bean plants was conducted during a little rainy period, inside a greenhouse, and under controlled conditions of temperature $\sim 27^\circ\text{C}$, and relative humidity of air $\sim 70\%$.

The Fe_3O_4 NPs, with a log-normal distribution of median diameter of ~ 10 nm and distribution width of ~ 0.36 , were prepared by the co-precipitation method described elsewhere (Rossi et al. 2007). Brown carbonated soils with 11.26 % of organic matter were used for the growth. The chemical and physical properties of the soil mixture were the following: loamy texture, pH of 7.3, 0.12 meq/100 g of assimilable phosphorus, 0.25 meq/100 g of potassium, 30–40 meq/100 g of cation exchange capacity, and 25–45 meq/100 g of base exchange capacity. According to the analysis performed on the soil mixture, plant nutrient levels were adequate for the growth of common bean plants (Fageria and Baligar 1999). We also mention that the soil used in our experiments, containing organic matter decomposition and nutrient cycling, may be classified as aerobic soil, i.e., it has a high concentration of oxygenated air to carry out oxidative reactions.

Plants were allowed to grow up until the vegetative stage V4 (Repinski et al. 2012). After 30 days, no toxicity on plants growth had been detected visually as well as no evidence of stubby roots and/or Fe deficiency in leaves. In fact, we have also observed that the roots were tiny and fibrous, i.e., prone to absorb water solutions from the soil. Then, plants of ~ 35 cm in height were removed from the polyethylene bags, rinsed well with deionized water, cut into short pieces, and subsequently dried at room temperature for fifteen days. After this step, each part of the plants was manually ground separately for about 30 min to form a fine powder for all characterizations. From each polyethylene bag, four samples were separated: soil (*S*), roots (*R*), stems (*T*), and leaves (*L*). For example, roots extracted from bags *B0*, *B1*, and *B2* were identified and labeled as samples *R0*, *R1*, and *R2*, respectively, as well as soils (*S0*, *S1*, and *S2*), stems (*T0*, *T1*, and *T2*), and leaves (*L0*, *L1*, and *L2*).

A multi-elemental analysis for 12 elements (B, Co, Mn, Mo, Ni, Zn, Ca, Fe, K, Mg, Na, and P) of each dried sample was performed in an inductively coupled plasma optical emission spectrometer (ICP-OES) Spectro Arcos (Spectro). Reference solutions with a high degree of analytical purity were used to obtain the calibration curves. Deionized water (Milli-Q) was used to prepare all solutions. All samples were subjected to microwave-assisted digestion in a Speed-wave Four microwave oven (Bergof) in a mixture of HNO_3 (2 mL), HF (2 mL), and H_2O_2 (1 mL). The samples were digested at 200°C for 15 min, 170°C for 10 min, and then 160°C for 5 min. The volume of the samples was then adjusted to 25 mL using deionized water before analysis.

All magnetization measurements were performed in a commercial Quantum Design SQUID magnetometer in powder samples. The magnetization as a function of temperature $M(T)$ was performed under both zero-field-cooled (ZFC) and field-cooled (FC) conditions. The ZFC cycle was performed after cooling down the sample to 5 K without the application of any magnetic field. After this step, a magnetic field of H_a was applied, and the data were collected by increasing the temperature from 5 to 300 K. Subsequently, the FC measurements were performed by cooling the sample slowly from 300 down to 5 K in the same applied magnetic field H_a . Also, the magnetic field dependence of the magnetization, $M(H)$, was measured in

the magnetic field range $-70 \leq H \leq 70$ kOe, and for selected temperatures of $T = 10$ and 300 K.

The magnetization data $M(T, H)$ were corrected in order to eliminate the intrinsic magnetic response of the plants. In plants irrigated with Fe_3O_4 NPs in aqueous solutions, the reported magnetization data as a function of temperature and applied magnetic field are described as:

$$M(T, H) = M_{\text{med}}(T, H) - M_{\text{control}}(T, H), \quad (1)$$

where $M_{\text{med}}(T, H)$ is the raw data measured in plants from bags $B1$ or $B2$, and $M_{\text{control}}(T, H)$ is the raw data measured in the control plant of bag $B0$. Assuming a superparamagnetic behavior of the magnetic moments (μ) at 300 K in roots, stems, and leaves of samples grown in bags $B1$ and $B2$, the field dependence of the magnetization follows the Langevin function weighted by a log-normal distribution ($f(\mu)$) (Fonseca et al. 2003):

$$M(H) = \frac{\int_0^\infty M_s \mathcal{L}\left(\frac{\mu H}{k_B T}\right) \mu f(\mu) d\mu}{\int_0^\infty \mu f(\mu) d\mu}, \quad (2)$$

where

$$f(\mu) = \frac{1}{\sqrt{2\pi}\mu\sigma_\mu} \exp\left(-\frac{\ln^2(\mu/\mu_0)}{2\sigma_\mu^2}\right), \quad (3)$$

μ_0 is the median magnetic moment, σ_μ the width of the magnetic moment distribution, M_s the saturation magnetization, $\mathcal{L}(x) = \coth x - 1/x$ the Langevin function, H the magnetic field, T the temperature, and k_B the Boltzmann constant. For spherical NPs, the median diameter (d_0) is obtained from $\mu_0 = M_s d_0^3 \pi / 6$, and the mean diameter from $\bar{d} = d_0 \exp(\sigma_d^2 / 2)$, where $\sigma_d = \sigma_\mu / 3$.

Results and discussion

ICP analysis: leaf concentrations of micronutrients

A brief approach to the leaf concentrations of micronutrients (LCM) B, Zn, Mn, Fe, Cu, and Mo is first presented here. The results obtained by using the ICP-OES technique were compared to the nutrient sufficiency ranges for the leaf of common bean plants reported in the literature (Reuter 1997). First, we have found that in leaf samples $L0$, $L1$, and $L2$, the ICP-OES

data indicated that values of B (~ 0.03 ppm), Zn (~ 0.02 ppm), Cu (~ 0.01 ppm), and Mo (~ 0.01 ppm) are all below their adequate range of values: (B) 25–70 ppm, (Zn) 35–60 ppm, (Cu) 8–30, and (Mo) 0.10–1.0 ppm (Reuter 1997). However, a different behavior has been observed for Mn and Fe concentrations, as indicated in Fig. 1 that displays the Mn and Fe leaf concentrations measured in samples $L0$, $L1$, and $L2$. The results indicate that the Mn leaf concentrations are 119.8, 107.5, and 134.6 ppm, respectively. All of these values are slightly higher than those considered adequate (from ~ 50 to ~ 100 ppm) for this element (Reuter 1997). On the other hand, the iron LCM in the three samples were ~ 186.1 , 201.4, and 263 ppm, respectively. Considering that the sufficient range for the leaf iron concentration in common bean plants is between 50 and 200 ppm (Reuter 1997), the ICP-OES data therefore indicate that the Fe content in the control sample $L0$ is slightly below the upper limit and may considered sufficient. The data also show that such a Fe concentration is slightly above the upper limit (200 ppm) in sample $L1$ and close to 30 % higher in sample $L2$. Combining the ICP-OES results for Fe and Mn, we point out that the ratio Fe/Mn in samples $L0$, $L1$, and $L2$ increases progressively with increasing Fe_3O_4 and were found to be 1.55, 1.87, and 1.97 in leaves $L0$, $L1$, and $L2$, respectively. The values of the ratio Fe/Mn are within the optimum range for common bean plants of 1.5–3 reported elsewhere (El-Jaoual and Cox 1998). As stated above, no visual toxicity or Fe deficiency was observed in all specimens studied. The obtained

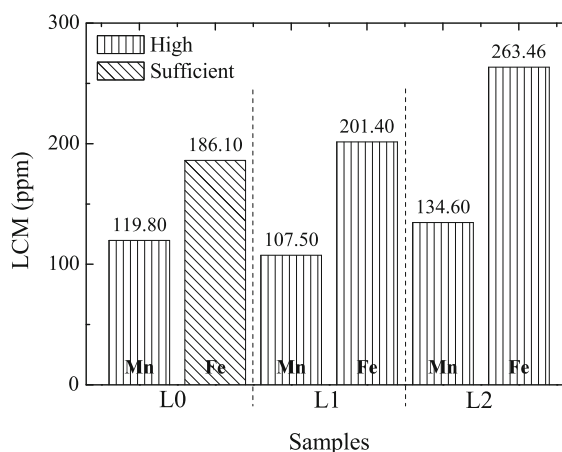


Fig. 1 Leaf concentrations of manganese (Mn) and iron (Fe) macronutrients in samples $L0$, $L1$, and $L2$

values for the Fe/Mn ratio in leaves, within the 1.55–1.97 range, give credence to the aforementioned statement.

The results displayed in Fig. 1 also indicate that increasing the concentration of Fe_3O_4 NPs in the soil results in an increase in Fe content in the plant aerial organs, i.e., an improvement in the uptake, translocation, and accumulation of Fe-based nutrients into the leaves. It is expected that this important and desired feature has its counterpart in the magnetic response of the plants irrigated with different concentrations of Fe_3O_4 nanoparticles, as discussed below.

Magnetization analysis

For a better understanding of the general magnetic behavior of the plants, we first analyze and discuss the magnetic behavior of the Fe_3O_4 NPs used in our study, as displayed in Fig. 2. The physical and magnetic properties of MNPs depend on several parameters as the size of the NPs and their size distribution, particle shape, anisotropy, the nature of the matrix in which the magnetic nanoparticles are embedded, the volume fraction of the magnetic material in a given specimen, and others (Leslie-Pelecky and Rieke 1996).

In systems comprised of monodisperse MNPs, the ZFC curves exhibit a maximum close to the so-called blocking temperature, T_B (Leslie-Pelecky and Rieke 1996), that depends on the volume and magnetic anisotropy of the NPs, applied and anisotropic

magnetic field, and measuring window time (see Fig. 2a). Above T_B , the MNPs are in the superparamagnetic state, where the magnetic moments behave as paramagnetic spins, and the system is in thermal equilibrium. Below T_B , the magnetic moments are in a blocked state and are unable to reach thermal equilibrium. Usually, the ZFC and FC curves coincide above the blocking temperature, but it occurs only at a certain irreversible temperature T_{ir} in polydisperse systems, as displayed in Fig. 2a. In almost all cases, systems comprised of NPs are polydisperse and the magnetic response of the whole sample is expressed as a sum over the contributions of individual NPs. Thus, the value of T_B and the width of the ZFC curve also depend strongly on the particle size distribution, as well as the concentration or volume fraction of the MNPs.

In $M(H)$ curves, the application of a sufficiently large magnetic field causes the magnetic moments within the sample to align with the magnetic field and the maximum value of the magnetization achieved in this state is termed saturation magnetization, M_s (see Fig. 2c). As the applied magnetic field decreases, the magnetic moments cease to be aligned with the field, and the total magnetization decreases to a remanent magnetization value, M_r , at zero applied field (see Fig. 2b). In order to bring the magnetization of the sample back to zero, a magnetic field with the magnitude of the coercive field, H_c , must be applied in the negative direction (see Fig. 2b). While $M(H)$ curves of MNPs taken well above T_B are reversible, with zero coercivity and remanence, as in ordinary paramagnets, they behave as in ferromagnetic materials below T_B , further exhibiting hysteresis, a feature accompanied by the occurrence of coercive fields, H_c , and remanent magnetization, M_r .

Figure 2a displays $M(T)$ curves measured under the application of a magnetic field of 500 Oe for Fe_3O_4 NPs. The curves resemble those of classical superparamagnetic systems, with $T_B \sim 130$ K and $T_{ir} \sim 220$ K. In addition, Fig. 2b, c shows the magnetic field dependence of the magnetization, $M(H)$, measured in Fe_3O_4 NPs at $T = 10$ K and $T = 300$ K, respectively. A small and linear contribution to the $M(H)$ data at high $H \geq 20$ kOe, probably due to surface effects and partial oxidation of the NPs, was subtracted from the raw data. The values of the saturation magnetization M_s are 82.8 and 68.5 emu/g at 10 and 300 K, respectively. Taking into consideration the

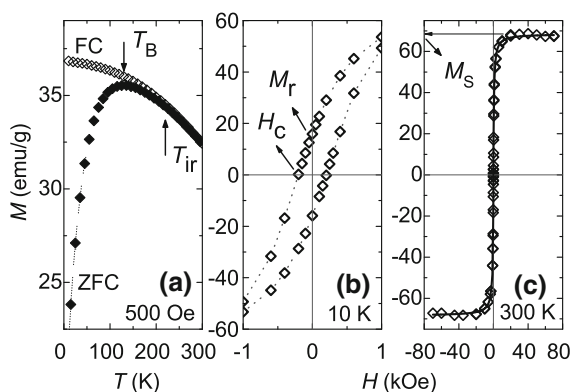


Fig. 2 Temperature dependence of the magnetization, $M(T)$, under zero-field-cooled (ZFC) and field-cooled (FC) conditions, of Fe_3O_4 nanoparticles (a). Magnetic field dependence of the magnetization, $M(H)$, at $T = 10$ K (b), and $T = 300$ K (c). Dotted lines are guides to the eyes, and solid lines are fitted curves using Eq. 2

subtraction made, the estimated values of M_s at both temperatures are in line with others in systems comprised of Fe_3O_4 NPs prepared by similar chemical routes (Barbeta et al. 2010).

The occurrence of a magnetic hysteresis, clearly observed in the $M(H)$ curve measured at 10 K, with $M_r \sim 16$ emu/g and $H_c \sim 200$ Oe, indicates that the MNPs are in the blocked state at low temperatures. On the other hand, at 300 K, only a small hysteresis in the $M(H)$ curve is observed, with $M_r = 0.9$ emu/g and $H_c \sim 10$ Oe. By considering the coercivity at 300 K negligible, we have fitted the $M(H)$ data by using Eq. 2. The dipolar interaction between Fe_3O_4 NPs was taken into account by adding a mean dipolar field inside the Langevin function. We obtained the mean diameter $\bar{d} = 6.7$ nm and the width of the size distribution $\sigma_d = 0.4$ for the Fe_3O_4 NPs. Nevertheless, the results from the magnetic characterization strongly suggest that Fe_3O_4 NPs used for the irrigation of the soils are mainly comprised of magnetic monodomain Fe_3O_4 NPs with a size distribution.

Magnetic behavior of soils

Figure 3 displays the magnetic characterization of the soil samples S0, S1, and S2. We first consider the temperature dependence of the magnetization, $M(T)$, displayed in Fig. 3a, and it is important to notice that the magnetic signal of the control sample S0 has been

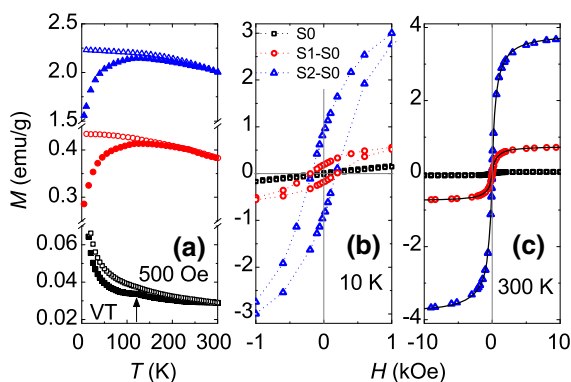


Fig. 3 **a** $M(T)$ curves measured under ZFC (closed symbols) and FC (opened symbols) conditions for soil samples S0, S1, and S2. The arrow indicates the temperature of the Verwey transition at ~ 125 K. **b** $M(H)$ curves measured at $T = 10$ K. **c** $M(H)$ curves at $T = 300$ K, after the subtraction of a small and linear contribution to $M(H)$ for high $H \geq 20$ kOe (see text for details). Dotted lines are guides to the eyes, and solid lines are fitted curves using Eq. 2

subtracted from the $M(T)$ data of samples S1[(S1 – S0)] and S2[(S2 – S0)]. We also mention that the $M(T)$ signal of the S0 sample is close to two orders of magnitude smaller than those measured in samples S1 and S2, as clearly observed in the figure. The $M(T)$ data show a small jump in the ZFC curve of the S0 sample at $T_v \sim 125$ K, a feature related to the Verwey transition, frequently observed in Fe_3O_4 , and associated with an abrupt change in the crystal structure of this material (Walz 2002). The ZFC magnetization signal of samples S1 and S2 are clearly larger than the magnetization of the S0 sample, and such a jump in the ZFC curves at $T_v \sim 125$ K is absent. The occurrence of the Verwey transition at $T_v \sim 125$ K in Fe_3O_4 NPs, such as observed in Fig. 3a, is expected in systems comprised of large NPs, usually with mean diameter ≥ 50 nm (Goya et al. 2003). Thus, from the data of Fig. 3a, it seems that our soil sample S0 contains large Fe_3O_4 particles, i.e., with mean diameter much larger than those of ~ 10 nm used in our study. On the other hand, the $M(T)$ data displayed in Fig. 3a for samples S1 and S2 are quite different and resemble the ones seen in the $M(T)$ data of tiny Fe_3O_4 NPs (see Fig. 2a). In fact, the ZFC curves of samples S1 and S2 exhibit a broad maximum centered at $T_B \sim 120$ K. Also, the temperature T_{ir} where the ZFC curve deviates from the FC one was found to be ~ 180 and 220 K for curves (S1 – S0) and (S2 – S0), respectively.

The $M(T)$ results indicate that the soil sample S0 contains a detectable amount of large Fe_3O_4 particles, and that samples S1 and S2 have enriched their magnetic volume fraction with tiny Fe_3O_4 NPs after the irrigation process, making an eventual signature of the Verwey transition in $M(T)$ curves absent. The data also suggest that the Fe_3O_4 NPs with the magnetite crystal phase and sizes similar to the pristine Fe_3O_4 NPs seem to be preserved in soil samples S1 and S2.

Figure 3b, c displays the $M(H)$ curves for samples S0, S1, and S2 measured at 10 and 300 K, respectively. The data clearly indicate that the remanence and coercivity of samples S0, S1, and S2 are higher at 10 K than at room temperature (see Table 1). At 10 K, M_r values were ~ 0.019 , 0.19 , and 0.89 emu/g for samples S0, S1, and S2, respectively. In addition, H_c increases with increasing Fe_3O_4 concentration and assumes values of ~ 100 , 195 , and 175 Oe, for the same samples, respectively. At 300 K, $M_r \sim 0.005$ emu/g for S0, 0.007 emu/g in sample S1, and 0.014 emu/g for S2. The results also showed that

Table 1 Some relevant parameters extracted from magnetic measurements: T_B is the blocking temperature, \bar{d} is mean NPs diameter, σ_d is the width of the size distribution, M_s is the saturation magnetization measured at $T = 300$ K, M_r is the remanent magnetization, and H_c is the coercivity

Samples	T_B (K)	\bar{d} (nm)	σ_d (nm)	M_s (10^{-3} emu/g)	M_r (10^{-3} emu/g)		H_c (Oe)	
					300 K	10 K	300 K	10 K
$S0$	—	—	—	49.6	19.3	4.6	100	58
$S1-S0$	120	7.5	0.3	747.1	190	7.3	195	2.5
$S2-S0$	120	7.4	0.4	3830	890	13.6	175	2.0
$R0$	—	—	—	3.3	1.1	0.6	180	280
$R1-R0$	120	7.1	0.3	56	13.9	0.8	160	8.3
$R2-R0$	130	7.4	0.3	86	19.2	0.7	158	5.4
$T0$	—	—	—	1.21	0.15	0.03	104	23
$T1-T0$	120	7.0	0.3	5.6	1.5	0.20	160	15
$T2-T0$	120	6.3	0.4	7.9	1.6	0.12	150	6.9
$L0$	—	—	—	1.2	0.13	0.05	90	40
$L1-L0$	105	7.7	0.3	2.4	0.98	0.05	211	2
$L2-L0$	120	6.0	0.4	3.7	1.1	0.02	150	2

$H_c \sim 60$, 2.5, and 2.0 Oe for samples S0, S1, and S2, respectively. The very high value of H_c at 300 K in sample S0 sustains the occurrence of large Fe_3O_4 particles in sample S0, a feature absent in samples S1 and S2, where $H_c \sim 2$ Oe, further indicating a super-paramagnetic behavior of the tiny Fe_3O_4 NPs at room temperature. The $M(H)$ data at 300 K and in the range of high magnetic fields were linear in field for all samples, probably due to weak antiferromagnetic/paramagnetic substances commonly found in soils. The subtraction of this linear contribution from the magnetization data leads to $M_s = 0.747$ and 3.83 emu/g for samples S1 and S2, respectively, indicating that the soil S2, with a higher Fe_3O_4 NPs concentration, displays a five times larger M_s when compared with the soil sample S1. From fittings of $M(H)$ curves of samples S1 and S2 to Eq. 2, we have found that $\bar{d} = 7.5$ and 7.4 nm, and $\sigma_d = 0.3$ and 0.4 in samples S1 and S2, respectively (see Table 1), which are very close to those obtained from the magnetization data of the Fe_3O_4 NPs. The values of \bar{d} agree well with the behavior of the $M(T)$ curves of samples S1 and S2 (see Fig. 3a) without any evidence of the Verwey transition close to 125 K, as expected for Fe_3O_4 NPs with $\bar{d} \leq 50$ nm (Goya et al. 2003).

The combined $M(T, H)$ results discussed here indicate that a high concentration of small Fe_3O_4 NPs, with mean diameter $\bar{d} \leq 50$ nm, is responsible for the magnetic behavior of samples S1 and S2, a feature hardly seen in the S0 sample, which is comprised of a small concentration of large Fe_3O_4 particles. These

features of samples S0, S1, and S2 are sufficient to explain many of the observations described above and the parameters listed in Table 1: (1) the occurrence of a well-defined signature of the Verwey transition in the $M(T)$ curve of sample S0; (2) the appreciable increase in M_s and M_r (at 300 K) and M_r and H_c (at 10 K) of samples S1 and S2; and (3) the large increase in the coercive field H_c , close to two times, in samples S1 and S2 at 10 K and a decrease of ~ 25 times at room temperature.

In the next subsections, the magnetic characterizations performed in different organs of the plants are presented separately. The magnetization $M(T, H)$ data were divided by the mass of each sample, and the strength of the magnetic signal is then related to the concentration of the magnetic material, i.e., in a first approximation, the higher the magnetic signal is, at a given temperature and applied magnetic field, the higher the concentration of MNPs will be.

Magnetic behavior of roots

In this and in the next two subsections, we address the magnetic properties of the three dried parts of the common bean plants: roots, stems, and leaves. The magnetic signals measured in these parts of the plants were at least two orders of magnitude smaller than those measured in soils (see Fig. 3; Table 1). The drastic decrease in the magnitude of the magnetic signal detected in roots, stems, and leaves is an expected result, in excellent agreement with the ones

discussed elsewhere (Zhu et al. 2008), where pumpkin seedlings were grown in hydroponic conditions. Thus, we start our discussion by describing the $M(T, H)$ data of the roots of samples grown in $B0$, $B1$, and $B2$ bags, as displayed in Fig. 4. We emphasize that the magnetization $M(T)$ data of the control sample $R0$ have been subtracted from the $M(T)$ signals of samples $R1[(R1 - R0)]$ and $R2[(R2 - R0)]$. The results in Fig. 4a indicate that the $M(T)$ curve of sample $R0$ is similar in some aspects to the $S0$ curve (see Fig. 3a), exhibiting features related to the Verwey transition in the ZFC branch of the $M(T)$ curves. Also, the magnetic signal of the $R0$ curve, as mentioned above, is close to two orders of magnitude smaller when compared to the one of the $S0$ samples. On the other hand, the $M(T)$ data of samples $R1$ and $R2$ are quite different from the one displayed in the $R0$ sample. We first mention that the Verwey transition, which is a clear signature in the $R0$ data, is absent in both $(R1 - R0)$ and $(R2 - R0)$ curves. We also mention that the concave downward curvature of the $M(T)$ data, seen in both $(R1 - R0)$ and $(R2 - R0)$ curves and typically observed in systems comprised of Fe_3O_4 NPs, is qualitatively different from the concave upward behavior of $M(T)$ reminiscent of the paramagnetic-like Curie law seen in $R0$ curves. In fact, the qualitative behavior of samples $R1$ and $R2$, very similar to the one observed in the Fe_3O_4

NPs (see Fig. 2a), exhibits a broad maximum centered at $T_B \sim 120$ and 130 K in ZFC curves, respectively (see Table 1). Also, the temperature in which the ZFC curve separates from the FC one was $T_{ir} \sim 136$ and 213 K for $R1$ and $R2$ samples, respectively.

The magnetization data displayed in Fig. 4b, c call our attention to important changes in the magnetic behavior of roots when compared, for instance, with the magnetic properties of the soils. Besides the almost two orders of magnitude decrease in the magnetic signals, we remark here that such a decrease is followed by drastic changes in the extracted magnetic parameters (M_s , M_r , and H_c) of the $M(H)$ data. For example, the magnetization saturation M_s at 300 K of samples $R1$ and $R2$ is ~ 17 and 25 times larger, respectively, than that estimated in sample $R0$. Also, the $M(H)$ curves of samples $R1$ and $R2$ exhibit a well-defined hysteresis at 10 K along with coercivity close to 180 in $R0$ and ~ 160 Oe in the two other samples $R1$ and $R2$. At room temperature, $H_c = 280$ Oe in sample $R0$, but is negligible in the $S1$ and $S2$ samples (see Table 1). The marked difference in the magnitude of H_c at 300 K indicates the presence of large Fe_3O_4 particles in the $R0$ sample, a feature hardly seen in samples $R1$ and $R2$ where the tiny Fe_3O_4 NPs are believed to display superparamagnetic behavior with negligible coercivity and remanent magnetization. After the subtraction of a small linear contribution to $M(H)$ curves at high magnetic fields due to diamagnetic substances in roots (Zhu et al. 2008), Eq. 2 was used to fit the curves for $(R1 - R0)$ and $(R2 - R0)$. From these fittings, we obtained $M_s = 5.6 \times 10^{-2}$ and 8.6×10^{-2} emu/g; $\bar{d} = 7.4$ and 7.1 nm; and $\sigma_d = 0.3$ for $(R1 - R0)$ and $(R2 - R0)$, respectively, in agreement with values obtained from the magnetization data for Fe_3O_4 NPs ($\bar{d} = 6.7$ nm and $\sigma_d = 0.4$). These combined results suggest that the higher the concentration of MNPs in soil is, the higher the absorption of nanoparticles by the roots will be at the concentration level of Fe_3O_4 NPs tested.

The magnetic characterization of samples $R1$ and $R2$ indicate that Fe_3O_4 nanoparticles are absorbed by the entire root system of common bean plants. Moreover, by comparing the $M(T, H)$ curves measured in pure NPs (see Fig. 2a) and roots (see Fig. 4a), it is possible to infer that the Fe_3O_4 particle size distribution in both samples is very similar and that the

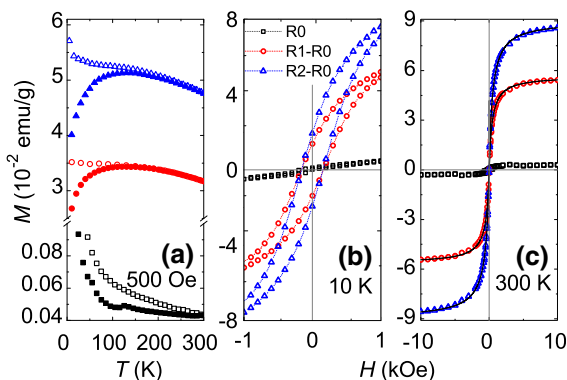


Fig. 4 **a** $M(T)$ curves measured under ZFC (closed symbols) and FC (opened symbols) conditions for root samples [curves $R0$, $(R1 - R0)$ and $(R2 - R0)$]. There is a break on y-axis separating two different magnetization ranges. **b** $M(H)$ curves measured at $T = 10$ K for $R0$, $(R1 - R0)$ and $(R2 - R0)$. Dotted lines are guides to the eyes. **c** $M(H)$ curves at $T = 300$ K for $R0$, $(R1 - R0)$, and $(R2 - R0)$, after the subtraction of a small and linear contribution to $M(H)$, as described in the text. Solid lines are fitted curves using Eq. 2

concentration of Fe_3O_4 NPs is larger in sample *R2*. We also argue that the magnetic behavior of the $M(T, H)$ data of samples *R1* and *R2* is dictated by the occurrence of tiny Fe_3O_4 NPs. These statements are supported by at least two features of the magnetic data: (1) the large increase in the M_s values at 300 K of samples *R1* and *R2*, being close to 17 and 25 times higher, respectively, than that of the control sample *R0*; and (2) the negligible values of H_c and M_r at 300 K, further indicating the occurrence of very small Fe_3O_4 nanoparticles within the root tissues.

Magnetic behavior of stems

From the discussion made above, it is clear that a significant amount of Fe_3O_4 NPs can be taken up by the common bean roots. The next step in our study is to verify whether the Fe_3O_4 NPs can be transported to the aerial parts of the plants, i.e., stems and leaves. Within this context, Fig. 5 displays the results of the magnetic characterization conducted in stems of the plants grown in bags *B0*, *B1*, and *B2*. Similarly from the above calculated values, the magnetic contribution of the control sample *T0* has been subtracted from the $M(T)$ signals of samples *T1*[(*T1* – *T0*)] and *T2*[(*T2* – *T0*)]. The set of the ZFC/FC curves for the stem samples, displayed in Fig. 5a, is similar to that

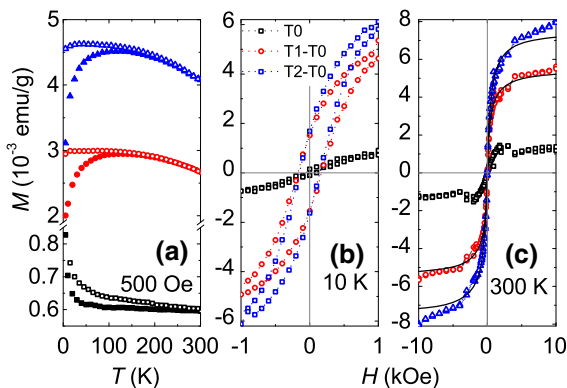


Fig. 5 $M(T)$ curves measured under ZFC (closed symbols) and FC (opened symbols) conditions for stem samples [curves *T0*, (*T1* – *T0*) and (*T2* – *T0*)]. There is a break on y-axis separating two different magnetization ranges. **b** $M(H)$ curves measured at $T = 10$ K for *T0*, (*T1* – *T0*) and (*T2* – *T0*). Dotted lines are guides to the eyes. **c** $M(H)$ curves at $T = 300$ K for *T0*, (*T1* – *T0*), and (*T2* – *T0*), after the subtraction of a small and linear contribution to $M(H)$ for, as described in the text. Solid lines are fitted curves using Eq. 2

observed in roots (see Fig. 4a) but with at least two important differences: (1) contrary to the observed in the root sample *R0*, the $M(T)$ curves of sample *T0* do not show any signature of the Verwey transition; and (2) the $M(T)$ curves of stem samples *T1* and *T2* have a similar qualitative behavior when compared with the one of Fe_3O_4 NPs (see Fig. 2a) and a slightly smaller magnitude of $M(T)$ when compared with samples *R1* and *R2* (see Fig. 4a). These results sustain that the magnetic contribution to $M(T)$ in stem samples *T1* and *T2* is associated with the presence of tiny Fe_3O_4 NPs, with $\bar{d} \leq 50$ nm, and that the concentration of Fe_3O_4 NPs in the stems is smaller than that of the roots. The occurrence of Fe_3O_4 NPs in samples *T1* and *T2* is further supported by similar features of their ZFC curves and those of the Fe_3O_4 NPs, as the broad maximum centered at $T_B \sim 120$ K (see Table 1) and $T_{ir} \sim 183$ and 215 K for (*T1* – *T0*) and (*T2* – *T0*), respectively.

The M versus H curves, measured in stem samples at 10 and 300 K, are shown in Fig. 5b, c, respectively. In both figures the magnetic signal of the sample *T0* is very little when compared to those from the stem samples *T1* and *T2*, following the same trend as observed in the root samples. Furthermore, the coercivity of samples *T1* and *T2* is large for the magnetic data taken at 10 K but negligible for those obtained at 300 K (see Table 1). After the subtraction of the linear contribution to the $M(H)$ curves, due to diamagnetic substances in the stems, Eq. 2 was used to fit the curves for (*T1* – *T0*) and (*T2* – *T0*) in Fig. 5c. We notice here that the raw data for *T0*, *T1*, and *T2* samples were slightly scattered in the high H range, making the subtraction of the small linear component to $M(H)$ more difficult than, for instance, those made in samples *R1* and *R2*. This is certainly related to different magnitudes of the weak magnetic signals arising from the stem samples which were collected at different distances from the roots. As discussed by (Zhu et al. 2008), stem samples close to roots exhibited magnetic signals at least two times larger than those close to the leaves. Our stem samples were comprised of a mixture of small pieces of stems from different distances from the roots, and the results displayed in Fig. 5 reflect an average value of the magnetic contribution. In any event, excellent fittings of the $M(H)$ data were obtained for magnetic fields up to ~ 5 kOe and the extrapolated values for higher fields resulted in $M_s = 5.6 \times 10^{-3}$ and

7.9×10^{-3} emu/g; $\bar{d} = 6.3$ and 7.0 nm; and $\sigma_d = 0.4$, and 0.3 , for samples $T1$ and $T2$, respectively, at room temperature. As observed in root samples, the magnetic characterization of the stem samples $T1$ and $T2$, with $H_c \sim 160$ Oe at 10 K, for instance, indicated that tiny Fe_3O_4 NPs were transported from the roots to the stems of the common bean plants.

Magnetic behavior of leaves

Following the data of roots and stems, the overall magnetic data for the leaf samples $L0$, $L1$, and $L2$ are displayed in Fig. 6. We first mention that the measured magnetic signals were slightly smaller than those of the stem samples, indicating a systematic and progressive decrease in the magnetic contribution to $M(T, H)$ data from the roots to the leaves. As in the early analyses, the magnetization of the control sample $L0$ has been subtracted from samples $L1[(L1 - L0)]$ and $L2[(L2 - L0)]$, and the temperature dependence of the magnetization for the three samples is shown in Fig. 6a. Once more, we have observed that the ZFC/FC curves of samples $L1(L1 - L0)$ and $L2(L2 - L0)$ resemble the magnetic behavior shown by the pure Fe_3O_4 NPs. Also, a broad maximum in the ZFC branch of the curves, centered at $T_B \sim 110$ and 120 K, respectively, is observed. We have also found that the temperature in which the ZFC curve separates from the FC one is $T_{ir} > 300$ and ~ 218 K for $(L1 -$

$L0)$ and $(L2 - L0)$, respectively. Similar to other parts of the plants studied, the control sample $L0$ exhibits a paramagnetic-like response in the ZFC/FC curves, a feature quite different when compared with those of samples $L1$ and $L2$. The $M(H)$ curves for samples $L0$, $L1(L1 - L0)$, and $L2(L2 - L0)$ measured at 10 and 300 K are displayed in Fig. 6b, c, respectively. The data shown in these figures clearly indicate that both remanence and coercivity develop in $(L1 - L0)$ and $(L2 - L0)$ curves. Furthermore, M_r and H_c follow the same trend as observed in roots and stems: they are larger at 10 K and assume very small values at 300 K (see Table 1). The magnitude of the magnetic signal in leaves from the irrigated plants with MNPs is at least four times larger than the control sample $L0$ at 10 and 300 K. Besides, after the subtraction of the linear contribution to $M(H)$ curves, Eq. 2 was used to fit curves $(L1 - L0)$ and $(L2 - L0)$ at 300 K and the results are shown in Fig. 6c. The fittings were of good quality, better than those obtained in the stem samples, due to the small magnitude of the magnetic signal. They resulted in $M_s = 2.4 \times 10^{-3}$ and 3.6×10^{-3} emu/g; $\bar{d} = 7.7$ and 6.0 nm; and $\sigma_d = 0.3$ and 0.4 for leaves $(L1 - L0)$ and $(L2 - L0)$, respectively. The results displayed in Fig. 6b, c indicate that the paramagnetic-like behavior observed in the $M(H)$ curves of samples $L1$ and $L2$ stems from very small Fe_3O_4 NPs accumulated in this part of the plants.

Fe_3O_4 NPs accumulation in the plant organs

Based on the results and discussion made above, we have demonstrated that different organs of common bean plants grown in soil can accumulate Fe_3O_4 NPs taken up from the soil. Additionally, we found that Fe_3O_4 NPs were absorbed by the roots, transported from the roots to stems and leaves, and accumulated in the plant aerial organs. In fact, the signature of the presence of Fe_3O_4 NPs in roots, stems, and leaves was inferred from similarities found in the magnetic characterization ($M(T, H)$ curves) of several samples, selected as representative of plant organs. For example, the $M(T, H)$ curves measured in roots, stems, and leaves displayed coercive fields H_c in the 150 – 211 and 0 – 15 Oe ranges, at 10 and 300 K, respectively (see Table 1). These values of H_c are very close to the ones measured in the Fe_3O_4 NPs used here (with mean diameter close to 10 nm and $H_c \sim 200$ and 10 Oe, at 10 and 300 K, respectively) and other Fe_3O_4 NPs with

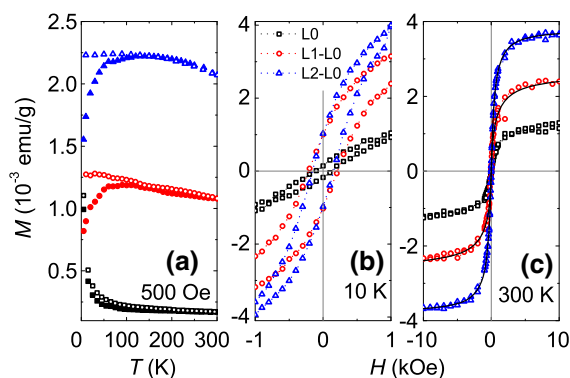


Fig. 6 $M(T)$ curves measured under ZFC (closed symbols) and FC (open symbols) conditions for leaf samples [curves $L0$, $(L1 - L0)$ and $(L2 - L0)$]. **b** $M(H)$ curves measured at $T = 10$ K for $L0$, $(L1 - L0)$ and $(L2 - L0)$. Dotted lines are guides to the eyes. **c** $M(H)$ curves at $T = 300$ K for $L0$, $(L1 - L0)$, and $(L2 - L0)$, after the subtraction of a small and linear contribution to $M(H)$ data at high values of H , as described in the text. Solid lines are fitted curves using Eq. 2

slightly different sizes (Goya et al. 2003; Lin et al. 2006). Also, from the fitting procedure to $M(H)$ data, by using Eq. 2, we have identified that the magnetic contribution to the magnetization of the three dried organs of the plants is closely related to a number of Fe_3O_4 NPs with mean diameter \bar{d} comprehended between 6.0 and 7.7 nm and σ_d between 0.3 and 0.4, as listed in Table 1. The mean diameter of the Fe_3O_4 NPs used in our study were estimated to be ~ 6.7 nm ($\sigma_d \sim 0.4$), further indicating the presence of tiny Fe_3O_4 NPs in roots, stems, and leaves.

We also want to point out that the measurement of magnetic signals arising from any organ of the plants may not be related specifically to stoichiometric Fe_3O_4 NPs. The high instability of tiny magnetite particles in air and/or water may cause a partial, superficial oxidation of the NPs leading to the occurrence of specimens with a core-shell morphology comprised of magnetite (core)-maghemite $\gamma\text{-Fe}_3\text{O}_4$ (shell) (Frison et al. 2013). If this were the case, further supported by the growth of the plants under aerobic soil conditions, one would expect: (1) a superficial oxidation of the Fe_3O_4 NPs due to a reaction with air and/or water in the soil and in other parts of the plants; (2) changes in the magnetic volume of both magnetic specimens, or more appropriately in the ratio of the volume fraction maghemite/magnetite. In fact, such a ratio has been found to increase when the Fe_3O_4 mean size decreases below 20 nm (Salazar et al. 2011), which could be the case here. Also, both features, the decrease in the Fe_3O_4 particle size and the increase in the maghemite/magnetite ratio would act to decrease significantly the Verwey transition temperature T_v , the blocking temperature T_B , and the saturation magnetization M_s (Goya et al. 2003; Salazar et al. 2011). In any event, our estimated values of the mean diameter \bar{d} of the pristine Fe_3O_4 NPs and the ones accumulated in soils and in different parts of the plants (roots, stems, and leaves) were found to vary little, being in a very narrow range between 6.0 and 7.7 nm, as discussed in the preceding paragraph and displayed in Table 1. In line with the very small change in the estimated values of \bar{d} , the blocking temperatures ($T_B \propto \bar{d}^3$), extracted from the ZFC branch of the $M(T)$ curves, were also found to vary in a narrow temperature window, from 105 to 130 K, in all specimens studied. All these findings indicate that the width of the maghemite shell, if present, may not changed

appreciably during the uptake, translocation, and accumulation of the Fe_3O_4 NPs by the plant organs. On the other hand, the progressive decrease in the saturation magnetization M_s from roots to leaves between samples of the same part of the plants is related to different concentrations of Fe_3O_4 NPs used during the irrigation in each case.

We turn now to the quantitative aspect of the $M(T, H)$ data and focus on the results of the saturation magnetization M_s at 300 K listed in Table 1. The M_s is closely related to the volume fraction of the magnetic material within the samples and we shall assume hereafter that contributions to M_s at 300 K only come from tiny Fe_3O_4 NPs. We first consider here some relationships between M_s at 300 K of samples from plants grown in bags *B1* and *B2* and the control plant from bag *B0*. The results show that ratios $[(R1 - R0)/R0] = 56/3.3 \sim 17$ and $[(R2 - R0)/R0] = 86/3.3 \sim 26$, i.e., indicate that the number of Fe_3O_4 NPs in the root sample *R2* is close to 50 % greater than *R1*. In fact, a similar increase of 50 % in the magnetic contribution was also observed when the stem samples *T2* and *T1*, $[(T1 - T0)/T0] = 5.6/1.2 \sim 4.6$ and $[(T2 - T0)/T0] = 7.9/1.2 \sim 6.5$, and the leaf samples *L2* and *L1*, $[(L1 - L0)/L0] \sim 2$ and $[(L2 - L0)/L0] \sim 3$, are considered. These results are compelling evidence in favor of the uptake of Fe_3O_4 NPs by the roots, their transport to stems and leaves, and their consequent accumulation in the plant organs. Also, at least for the Fe_3O_4 NPs concentration levels used, the estimate magnetic volume in roots, stems, and leaves was observed to increase accordingly with increasing magnetic concentration of the water solutions used during the irrigation.

The magnetic results discussed here can also be transformed in number (N) of Fe_3O_4 NPs/g accumulated by the plant organs. Firstly, by assuming $M_s = 68.5$ emu/g at 300 K for the pure Fe_3O_4 NPs, with $\bar{d} \sim 10$ nm, and density of $\rho = 5.2$ g/cm³ (Cullity and Graham 2011), the magnetic moment of an individual Fe_3O_4 NP (μ_{NP}) is obtained by

$$\mu_{\text{NP}} = M_s \rho \frac{\pi}{6} d^3. \quad (4)$$

Finally, the number of Fe_3O_4 in plant organs is estimated by using the expression

$$N = \frac{M_s^{\text{plant}}}{\mu_{\text{NP}}}, \quad (5)$$

where M_s^{plant} is the M_s values of plant organs listed in Table 1. We have estimated that leaves of the plants grown in bags B1 and B2 have 1.3 and 2.0×10^{13} Fe_3O_4 NPs/g, respectively. In both plants, $\sim 4\%$ of Fe_3O_4 NPs are detected in their leaves, $\sim 8\%$ in their stems, and $\sim 88\%$ in their roots.

Conclusions

In summary, we were able to grow common bean plants in soil which were irrigated with water solutions containing different concentrations of Fe_3O_4 NPs. No toxicity on plant growth has been detected visually as well as no evidence of Fe deficiency in leaves were detected at the concentrated levels of Fe_3O_4 NPs studied, as inferred from the inductively coupled plasma optical emission spectrometry results performed in roots, stems, and leaves. On the other hand, our temperature and magnetic field dependence of the magnetization $M(T, H)$ data indicate a progressive and systematic increase in the magnetization signal in leaves, stems, and root samples of plants grown in soils irrigated with increasing concentration of Fe_3O_4 NPs suspensions. From the extracted parameters of $M(T, H)$ curves such as saturation magnetization, M_s , coercive field, H_c , and remanent magnetization, M_r , we were able to conclude that Fe_3O_4 NPs are uptaken by the roots, transported throughout the plant parts, and accumulated in the plant organs. Also, the similarities observed in H_c and M_r values extracted from different parts of the plants lead us to identify that Fe_3O_4 NPs were responsible for the magnetic contribution to the $M(T, H)$ signals in a wide range of temperature and applied magnetic field. Such a feature was used for estimating the number of Fe_3O_4 NPs/g in roots, stems, and leaves. We have found that the concentration of Fe_3O_4 NPs is close to 0.64×10^{13} Fe_3O_4 NPs/g in the control plant, a number that increases from 1.3 to 2.0×10^{13} Fe_3O_4 NPs/g in leaves L1 and L2, respectively. We demonstrate that a large amount of tiny Fe_3O_4 NPs in soil medium can be taken up by common bean plants, translocated to their aerial parts, and accumulated in the plant organs.

Acknowledgments The authors acknowledge the financial support provided by Brazil's agencies Fundação de Amparo à Pesquisa do Estado de São Paulo (FAPESP) (Grant Nos.

2014/12392-3, 2014/19245-6, and 2013/07296-2) and Conselho Nacional de Desenvolvimento Científico e Tecnológico (CNPq) (Grant Nos. 168255/2014-6, 444712/2014-3, 501446/2014-1, and 308706/2007-2).

References

- Arruda SCC, Silva ALD, Galazzi RM, Azevedo RA, Arruda MAZ (2015) Nanoparticles applied to plant science: a review. *Talanta* 131:693–705. doi:10.1016/j.talanta.2014.08.050. <http://www.sciencedirect.com/science/article/pii/S0039914014007309>
- Barbeto VB, Jardim RF, Kiyohara PK, Effenberger FB, Rossi LM (2010) Magnetic properties of Fe_3O_4 nanoparticles coated with oleic and dodecanoic acids. *J Appl Phys* 107(7):073913. doi:10.1063/1.3311611
- Barrena R, Casals E, Colón J, Font X, Sánchez A, Puntès V (2009) Evaluation of the ecotoxicity of model nanoparticles. *Chemosphere* 75(7):850–857. doi:10.1016/j.chemosphere.2009.01.078
- Barrios AC, Rico CM, Trujillo-Reyes J, Medina-Velo IA, Peralta-Videa JR, Gardea-Torresdey JL (2016) Effects of uncoated and citric acid coated cerium oxide nanoparticles, bulk cerium oxide, cerium acetate, and citric acid on tomato plants. *Sci Total Environ* 563564:956–964. doi:10.1016/j.scitotenv.2015.11.143. <http://www.sciencedirect.com/science/article/pii/S0048969715311244>
- Broughton WJ, Hernández G, Blair M, Beebe S, Gepts P, Vanderleyden J (2003) Beans (*Phaseolus* spp.)—model food legumes. *Plant Soil* 252(1):55–128. doi:10.1023/A:1024146710611
- Carpita NC, Gibeau DM (1993) Structural models of primary cell walls in flowering plants: consistency of molecular structure with the physical properties of the walls during growth. *Plant J* 3(1):1–30
- Chen H, Seiber JN, Hotze M (2014) ACS select on nanotechnology in food and agriculture: a perspective on implications and applications. *J Agric Food Chem* 62(6):1209–1212. doi:10.1021/jf5002588
- Corredor E, Testillano PS, Coronado MJ, González-Melendi P, Fernández-Pacheco R, Marquina C, Ibarra MR, de la Fuente JM, Rubiales D, Pérez-de Luque A, Risueño MC (2009) Nanoparticle penetration and transport in living pumpkin plants: in situ subcellular identification. *BMC Plant Biol* 9(1):45–56
- Cullity BD, Graham CD (2011) Introduction to magnetic materials, 2nd edn. Wiley, New York
- El-Jaoual T, Cox DA (1998) Manganese toxicity in plants. *J Plant Nutr* 21(2):353–386. doi:10.1080/01904169809365409
- Fageria NK, Baligar VC (1999) Growth and nutrient concentrations of common bean, lowland rice, corn, soybean, and wheat at different soil pH on an inceptisol. *J Plant Nutr* 22(9):1495–1507. doi:10.1080/01904169909365730
- Fleischer A, O'Neill MA, Ehwald R (1999) The pore size of non-graminaceous plant cell walls is rapidly decreased by borate ester cross-linking of the pectic polysaccharide rhamnogalacturonan II. *Plant Physiol* 121(3):829–838
- Fonseca F, Goya G, Jardim R, Carreño N, Longo E, Leite E, Muccillo R (2003) Magnetic properties of $\text{Ni}:\text{SiO}_2$ nanocomposites synthesized by a modified sol–gel method.

- Appl Phys A 76(4):621–623. doi:[10.1007/s00339-002-2029-9](https://doi.org/10.1007/s00339-002-2029-9)
- Frison R, Cernuto G, Cervellino A, Zaharko O, Colonna GM, Guagliardi A, Masciocchi N (2013) Magnetite–maghemite nanoparticles in the 5–15 nm range: correlating the core–shell composition and the surface structure to the magnetic properties. A total scattering study. Chem Mater 25(23):4820–4827. doi:[10.1021/cm403360f](https://doi.org/10.1021/cm403360f)
- Goya G, Berquo T, Fonseca F, Morales M (2003) Static and dynamic magnetic properties of spherical magnetite nanoparticles. J Appl Phys 94(5):3520–3528
- Graham R, Welch R (1999) A new paradigm for world agriculture: productive, sustainable and nutritious food systems to meet human needs. Dev Bull (Canberra) 49:29–32
- Grusak MA (2002) Enhancing mineral content in plant food products. J Am Coll Nutr 21(sup3):178S–183S. doi:[10.1080/07315724.2002.10719263](https://doi.org/10.1080/07315724.2002.10719263)
- Kurepa J, Paunesku T, Vogt S, Arora H, Rabatic BM, Lu J, Wanzer MB, Woloschak GE, Smalle JA (2010) Uptake and distribution of ultrasmall anatase TiO Alizarin red S nanoconjugates in *Arabidopsis thaliana*. Nano Lett 10(7):2296–2302. doi:[10.1021/nl903518f](https://doi.org/10.1021/nl903518f)
- Leslie-Pelecky DL, Rieke RD (1996) Magnetic properties of nanostructured materials. Chem Mater 8(8):1770–1783. doi:[10.1021/cm960077f](https://doi.org/10.1021/cm960077f)
- Lin CR, Chiang RK, Wang JS, Sung TW (2006) Magnetic properties of monodisperse iron oxide nanoparticles. J Appl Phys 99(8):08N710. doi:[10.1063/1.2172891](https://doi.org/10.1063/1.2172891)
- Lin D, Xing B (2008) Root uptake and phytotoxicity of zno nanoparticles. Environ Sci Technol 42(15):5580–5585. doi:[10.1021/es800422x](https://doi.org/10.1021/es800422x)
- López-Luna J, Silva-Silva M, Martínez-Vargas S, Mijangos-Ricardez O, González-Chávez M, Solís-Domínguez F, Cuevas-Díaz M (2016) Magnetite nanoparticle (NP) uptake by wheat plants and its effect on cadmium and chromium toxicological behavior. Sci Total Environ 565:941–950. doi:[10.1016/j.scitotenv.2016.01.029](https://doi.org/10.1016/j.scitotenv.2016.01.029). <http://www.sciencedirect.com/science/article/pii/S0048969716300298>
- López-Moreno ML, Avilés LL, Pérez NG, Álamo Irizarry B, Perales O, Cedeno-Mattei Y, Román F (2016) Effect of cobalt ferrite (CoFe₂O₄) nanoparticles on the growth and development of *Lycopersicon lycopersicum* (tomato plants). Sci Total Environ 550:45–52. doi:[10.1016/j.scitotenv.2016.01.063](https://doi.org/10.1016/j.scitotenv.2016.01.063)
- Maurer-Jones MA, Gunsolus IL, Murphy CJ, Haynes CL (2013) Toxicity of engineered nanoparticles in the environment. Anal Chem 85(6):3036–3049. doi:[10.1021/ac303636s](https://doi.org/10.1021/ac303636s)
- Navarro E, Baun A, Behra R, Hartmann NB, Filser J, Miao AJ, Quigg A, Santschi PH, Sigg L (2008) Environmental behavior and ecotoxicity of engineered nanoparticles to algae, plants, and fungi. Ecotoxicology 17(5):372–386
- Repinski SL, Kwak M, Gepts P (2012) The common bean growth habit gene PvTFL1y is a functional homolog of arabidopsis TFL1. Theor Appl Genet 124(8):1539–1547. doi:[10.1007/s00122-012-1808-8](https://doi.org/10.1007/s00122-012-1808-8)
- Reuter DJ (1997) Plant analysis: an interpretation manual, 2nd edn. CSIRO Publishing, Clayton
- Rico CM, Majumdar S, Duarte-Gardea M, Peralta-Videa JR, Gardea-Torresdey JL (2011) Interaction of nanoparticles with edible plants and their possible implications in the food chain. J Agric Food Chem 59(8):3485–3498. doi:[10.1021/jf104517j](https://doi.org/10.1021/jf104517j)
- Roberts A, Oparka K (2003) Plasmodesmata and the control of symplastic transport. Plant Cell Environ 26(1):103–124
- Roppolo D, De Rybel B, Tendon VD, Pfister A, Alassimone J, Vermeer JE, Yamazaki M, Stierhof YD, Beeckman T, Geldner N (2011) A novel protein family mediates casparian strip formation in the endodermis. Nature 473(7347):380–383
- Rossi LM, Vono LL, Silva FP, Kiyohara PK, Duarte EL, Matos JR (2007) A magnetically recoverable scavenger for palladium based on thiol-modified magnetite nanoparticles. Appl Catal A 330:139–144. doi:[10.1016/j.apcata.2007.07.018](https://doi.org/10.1016/j.apcata.2007.07.018)
- Salazar JS, Perez L, de Abril O, Phuoc LT, Ihiwakrim D, Vazquez M, Greneche JM, Begin-Colin S, Pourroy G (2011) Magnetic iron oxide nanoparticles in 10–40 nm range: composition in terms of magnetite/maghemite ratio and effect on the magnetic properties. Chem Mater 23(6):1379–1386. doi:[10.1021/cm103188a](https://doi.org/10.1021/cm103188a)
- Schiavo S, Oliviero M, Miglietta M, Rametta G, Manzo S (2016) Genotoxic and cytotoxic effects of ZnO nanoparticles for *Dunaliella tertiolecta* and comparison with SiO₂ and TiO₂ effects at population growth inhibition levels. Sci Total Environ 550:619–627. doi:[10.1016/j.scitotenv.2016.01.135](https://doi.org/10.1016/j.scitotenv.2016.01.135)
- Schwab F, Zhai G, Kern M, Turner A, Schnoor JL, Wiesner MR (2016) Barriers, pathways and processes for uptake, translocation and accumulation of nanomaterials in plants critical review. Nanotoxicology 10(3):257–278. doi:[10.3109/17435390.2015.1048326](https://doi.org/10.3109/17435390.2015.1048326)
- Servin A, Elmer W, Mukherjee A, De la Torre-Roche R, Hamdi H, White JC, Bindran P, Dimkpa C (2015) A review of the use of engineered nanomaterials to suppress plant disease and enhance crop yield. J Nanopart Res 17(2):1–21. doi:[10.1007/s11051-015-2907-7](https://doi.org/10.1007/s11051-015-2907-7)
- Walz F (2002) The verwey transition—a topical review. J Phys Condens Matter 14(12):R285
- Wang TL, Domoney C, Hedley CL, Casey R, Grusak MA (2003) Can we improve the nutritional quality of legume seeds? Plant Physiol 131(3):886–891
- Welch RM, Graham RD (1999) A new paradigm for world agriculture: meeting human needs: productive, sustainable, nutritious. Field Crops Res 60(1–2):1–10. doi:[10.1016/S0378-4290\(98\)00129-4](https://doi.org/10.1016/S0378-4290(98)00129-4)
- Welch RM, Graham RD (2004) Breeding for micronutrients in staple food crops from a human nutrition perspective. J Exp Bot 55(396):353–364. doi:[10.1093/jxb/erh064](https://doi.org/10.1093/jxb/erh064)
- Zahra Z, Arshad M, Rafique R, Mahmood A, Habib A, Qazi IA, Khan SA (2015) Metallic nanoparticle (TiO₂ and Fe₃O₄) application modifies rhizosphere phosphorus availability and uptake by *Lactuca sativa*. J Agric Food Chem 63(31):6876–6882. doi:[10.1021/acs.jafc.5b01611](https://doi.org/10.1021/acs.jafc.5b01611)
- Zhu H, Han J, Xiao JQ, Jin Y (2008) Uptake, translocation, and accumulation of manufactured iron oxide nanoparticles by pumpkin plants. J Environ Monit 10:713–717. doi:[10.1039/B805998E](https://doi.org/10.1039/B805998E)